Histol Histopathol (2019) 34: 1073-1088

http://www.hh.um.es

Histology and Histopathology

From Cell Biology to Tissue Engineering

Adult-onset Alexander disease with a heterozygous D128N GFAP mutation: a pathological study

Juan José Cabrera-Galván[1,2,4], María Soledad Martínez-Martin[1,2], Daniel Déniz-García[2], Eduardo Araujo-Ruano[2] and María del Mar Travieso-Aja[3]

[1]Pathological Anatomy Service, Maternal and Insular Hospital Complex of the Canary Health Service (SCS), [2]Pathology Unit, Morphology Department, Las Palmas de Gran Canaria University (ULPGC), [3]Department of Radiology, Hospital Group San Roque and [4]Instituto Universitario de Investigaciones Biomédicas y Sanitarias (IUIBIS), Las Palmas de Gran Canaria, Spain

Summary. The various forms of Alexander disease (AD) have been linked to heterozygous point mutations in the coding region of the *Human glial fibrillary acidic protein* (*GFAP*) gene. The aim of this study was to confirm and characterise an adult variant of AD based on the presence of Rosenthal fibres, which were identified at brain autopsy.

We performed histological and immunohistochemical studies and mutation screening by cycle sequencing of exons 1, 4, 6, and 8. A heterozygous D128N *GFAP* mutation, previously described in three other cases of adult-onset AD (AOAD), was genetically confirmed. The mutation was seemingly sporadic. Symptoms of the female, 65-year-old patient started with occasionally asymmetric motor impairment and concluded, 23 months later, with a lack of spontaneous movement in all four limbs, reduced consciousness, an acute respiratory problem, and eventually lethal exitus. The most striking characteristics were a cerebellar syndrome with subsequent clinical signs due to brainstem and spinal cord involvement. The final diagnosis was based on a complete autopsy, detection of Rosenthal fibres, GFAP, vimentin, alpha B-crystallin, ubiquitin, hsp27, neurofilament, and synaptophysin, and the identification of the corresponding *GFAP* gene mutation. Blood analyses were positive for ANA and rheumatoid factor.

In conclusion, this work describes sporadic, rapidly advancing AOAD in a female patient and links it with other published cases with the same mutation. Reflections are provided on the influence of vasculitis and ANA in AD as well as the presence of Rosenthal fibres in the neurohypophysis.

Key words: Alexander disease, D128N *GFAP* mutation, Immunohistochemistry, MRI, Pathology

Offprint requests to: Juan J. Cabrera-Galván, Pathology Unit, Morphology Department, Faculty of Health Sciences, ULPGC, Blas Cabrera Felipe s/n, 35016 Las Palmas de Gran Canaria, Spain. e-mail: juanjose.cabrera@ulpgc.es

DOI: 10.14670/HH-18-110

Introduction

Alexander disease (AD), originally described by Alexander WS (Alexander, 1949), is a rare, neurological disease characterised by a pattern of leukodystrophy with gliosis, diffuse demyelination, and the presence of Rosenthal fibres.

Classically, AD has been divided into three subtypes according to the age of onset, an infantile, a juvenile, and an adult form with an occurrence frequency of 27.3%, 24.2%, and 48.5%, respectively. The categories cerebral (Type 1), bulbospinal (Type 2), and intermediate (Type 3) AD have been proposed as a simplified, clinical guideline (Yoshida et al., 2011). Due to the challenge regarding classification, Prust et al. (2011) suggested only two forms. Type I, related to early childhood around the age of four, is accompanied by seizures, macrocephaly, encephalopathy, failure to thrive, developmental delay, and classic magnetic resonance imaging (MRI) signs. Type II occurs in older children and adults throughout life. It encompasses familial as well as sporadic forms and the most variable clinical manifestations, like autonomic

dysfunction, an affected brainstem, bulbar and spinal cord junction, dysarthria, dysphagia, dysphonia, nystagmus, and pyramidal tract involvement, cerebellar ataxia, palatal myoclonus, and atypical MRI features. Type II AD frequently lacks neurocognitive symptoms or developmental deficits (Brenner et al., 2001; Pareyson et al., 2008; Prust et al., 2011).

MRI of infantile cases shows signal abnormalities in the cerebral white matter, mainly in the frontal regions, which led to the proposal of five criteria for an MRI-based diagnosis of AD (van der Knaap et al., 2001). However, according to Farina et al. (2008), MRI that shows a progressive atrophy of the medulla oblongata and upper cervical spinal cord C1–C2 with hyperintensities on T2-weighted images is highly suggestive of adult-onset AD (AOAD).

Other signs, such as a tadpole-like brainstem atrophy with medulla oblongata and cervical spinal cord atrophy, are observed in adult AD (Namekawa et al., 2010). Therefore, MRI is basic to diagnose AOAD. Incidentally detected MRI findings, consisting of upper cervical cord, medulla oblongata and cerebellum atrophy gave rise to a proposed AOAD diagnosis even without apparent family history or symptoms in the patient and point out the key role of genetic GFAP testing for confirmation (Sugiyama et al., 2015).

A common, neuropathological feature, used as a histopathological, diagnostic hallmark of AD, is the diffuse presence of Rosenthal fibres. When stained with eosin and studied by light microscopy, these intracytoplasmic aggregations within astrocytes and their processes appear as round or elongated hyaline bodies (Brenner et al., 2001). They contain GFAP, the main intermediate filament of astrocytes, as well as cellular stress proteins such as hsp27, alpha B-crystallin, and ubiquitin (Iwaki et al., 1993; Wippold et al., 2006, Quinlan et al., 2007). In addition, gliosis accompanied by astrocyte hypertrophy as well as a decrease in astrocyte numbers and degeneration of the white matter with a variable degree of neuron loss are consistently observed. Consequently, astrocyte alterations may affect the other cell types (Sosunov et al., 2018).

Further intermediate filaments poorly studied in AD, e.g. vimentin, have been associated with GFAP as copolymers in cases of reactive astrocytosis and in glioma cell lines (Pixley and Vellis, 1984; Reeves et al., 1989; Pekny et al., 2014). Synaptophysin, an integral membrane glycoprotein in the presynaptic vesicles of almost all neurons, and the phosphorylated neurofilaments have been used as immunohistochemical targets in axons and nerve fibres to understand the pathogenesis of neurological diseases. Thus, synaptophysin has been described as a marker of axonal damage in experimental models of demyelination and neuroinflammatory lesions (Gudi et al., 2017). Chang et al. (2015) incorporated phosphorylated neurofilament proteins in their study on AD, as their thickening also indicates axonal damage.

Finally, lymphocytes around blood capillaries of the brainstem have been described in AD and related to a possible inflammatory status (Olabarria et al., 2015; Sosunov et al., 2018).

De novo mutations occur in infantile AD, while sporadic, familiar, as well as *de novo* cases have been described for the adult forms. The genetic study of GFAP mutations is necessary to understand the pathogenesis, the type of disease, and the manifestations of AD (Messing et al., 2001). Dominant missense mutations account for practically all forms of the disease and translate into changes in the capacity to form filaments. Precipitates and aggregates involving the small heat shock proteins hsp27 and alpha B-crystallin add to form Rosenthal fibres through a gain-of–function mechanism, which could explain AOAD pathogenesis (Li et al., 2002, 2005; Quinlan et al., 2007; Sosunov et al., 2017).

The rare mutation GFAP c.382 G>A (p.D128N) had been described by Pareyson et al. (2008) and Farina et al. (2008) in a 62-year-old patient with limb weakness, spasticity, pyramidal signs, abnormal gait, but no signs of ataxia, and an onset of disease two years before diagnosis. They observed atrophy and changes in the MRI intensity of the medulla oblongata and upper cervical cord, whereas the supratentorial region and periventricular zones were free of alterations. However, 8 out of the 11 studied patients exhibited cerebellar changes (Farina et al., 2008; Pareyson et al., 2008).

Chang et al. (2015) described the same mutation in a 52-year-old male with paraplegia, three years since disease onset, and an MRI revealing severe atrophy of the distal brainstem and spinal cord. At autopsy, middle to moderate atrophy of the cerebrum, cerebellum, and brainstem were observed as well as a greyish discolouration in the white matter. The histopathological study revealed foci of demyelination and periventricular Rosenthal fibres in the cerebellum, pons, and hippocampus.

Recently, Lee et al. (2017) described this mutation in a case of a 68-year-old man, only months since onset, with slowly progressing gait disturbance and a tendency to fall, ataxia, dysphagya, dysarthria, bilateral, gaze-evoked nystagmus, and deep tendon reflexes, all of which indicated dysfunction in the brainstem, cerebellum, or cervical cord. MRI showed marked atrophy of the medulla oblongata and upper cervical cord, mild atrophy of the cerebellar hemisphere on both sagittal T2- and T1-weighted images, and hyperintense lesions in the bilateral dentate nuclei in FLAIR sequences, all suggestive of AOAD (Lee et al., 2017).

To our knowledge, the mutation described in the present work had only been detected in adult patients. In contrast to the aforementioned works, the aim of this study was to establish a diagnosis of AD based on a complete autopsy and histological study.

Materials and methods

The hospital ethics committee approved the study,

and family consent was obtained.

Following a macroscopic autopsy study, tissue from selected visceral areas was fixed in 10% buffered formaldehyde. The brain was fixed the same way, and pathological areas were selected from the brain stem, cerebellum, and spinal cord. All the material was embedded in paraffin, cut into 4 µm sections, and stained with haematoxylin and eosin (H&E), periodic acid-Schiff (PAS) stain, and Kluver-Barrera stain for myelin visualisation.

Immunohistochemical procedures

Sections were deparaffinised and then progressively hydrated until PBS. Heat-induced antigen retrieval was performed, followed by inhibition of the endogenous peroxidase for 15 min. Thereafter, sections were incubated with the following primary antibodies for 30 min at room temperature: anti-vimentin (monoclonal mouse anti-human, clone V9, DakoCytomation, Carpinteria, Ca, USA; dilution 1:400), anti-GFAP (polyclonal rabbit anti-glial fibrillary acidic protein Z 0334, DakoCytomation; 1:100), anti-neurofilament (monoclonal mouse anti-human neurofilament protein, clone 2F11, DakoCytomation; 1:200), anti-synaptophysin (polyclonal rabbit anti-human synaptophysin DakoCytomation; 1:200), anti-alpha B-crystallin (monoclonal mouse anti-human, Clone: F-10, Gennova Scientific, Spain; 1:100), anti-ubiquitin (polyclonal rabbit anti-human, Gennova Scientific; 1:50), anti-hsp27 (monoclonal mouse anti-human, Gennova Scientific, 1:200). Negative controls were performed replacing the primary antibody by PBS. Thereafter, the sections were incubated with the Chenmate Dako Envision Detection Kit Peroxidase/DAB® and finally counterstained with Harris haematoxylin for 30 s, dehydrated, and mounted in DPX with coverslips. Intensity of immunohistochemical staining was graded on a semi-quantitative scale as absent, weak to moderate, or strong.

Molecular techiques

A mutation screening was performed on genomic DNA extracted from formalin-fixed and paraffin-embedded tissue from brain samples. Control samples came from four healthy subjects. To screen for a possible AOAD-causing mutation in the *GFAP* gene, exons 1, 4, 6, and 8, which cover 97% of the most likely mutations, were subjected to cycle sequencing (ABI PRISM Dye Terminator Cycle Sequencing Kit, Applied Biosystems, Foster City, Ca, USA) and analysis was performed on an ABI PRISM 310 Genetic Analyser (Applied Biosystems, Waltham, Ma, USA). PCR primer sequences are given in Table 1.

Data was analysed using the BioEdit sequence alignment software 7.2.1.

Literature search strategies included PubMed database up to November, 2018, applying the search terms "Alexander disease" and "GFAP", and the mutation database of the Waisman Center at http://waisman.wisc.edu/alexander/.

Results

Clinical findings and MRI data

The patient, a 65-year-old woman with a hypertension history was admitted to hospital for cerebellar syndrome of no related cause, characterised by a general, neurological, chronic and progressive deterioration, cerebellar ataxia, and progressive dysarthria, but no evidence of palatal myoclonia.

A year and a half before and after stent implantation in the left renal and right femoral artery, she began to lose vitality, showed little interest in things, felt instability on cephalic turns, walked with difficulty, suffering frequent falls, and spoke slowly with difficulty in articulating words.

On clinical neurological examination, the patient was conscious, oriented, and without apparent cognitive deficit. She exhibited ataxic gait and difficulty in the tandem test, cephalic and bilateral distal tremor in the limbs, particularly in the upper limbs, which increased with exercise (intention tremor), and an inexhaustible, bilateral, horizontal-rotatory nystagmus. She had not lost strength in her four limbs and preserved the symmetrical muscle reflexes (osteotendinous reflexes and cutaneous plantar response) and normal sensitivity.

The remaining examination did not reveal further abnormalities. The blood test was normal, except for a rheumatoid factor (RF) of 51 IU/mL (normal range: 15-20 IU/mL). The cerebrospinal fluid was unremarkable, with a normal level of immunoglobulins, negative for herpes viruses I and II, and cytomegalovirus. The cytological study did not lead to any findings.

A cranial, T2-weighted MRI showed diffuse and

Table 1. GFAP primers for DNA cycle sequencing of exons 1, 4, 6, and 8.

	FORWARD PRIMER	REVERSE PRIMER
EXON 1	5´ATGGAGAGGAGACGCATCA3´	5´CCTCCTCACTTCTGCCTCAC3´
EXON 4	5´CTCACCCTGGTCAGGAGGT3´	5´AGGCAGGGCTACCTTGGAG3´
EXON 6	5´GAGTCCCTGGAGAGGCAGAT3´	5´GAGGCAGCAGGGAGACTTC3´
EXON 8	5´GGGCATGGGAGAGGATG3´	5´GGCCTGGCCTTGAGAATC3´

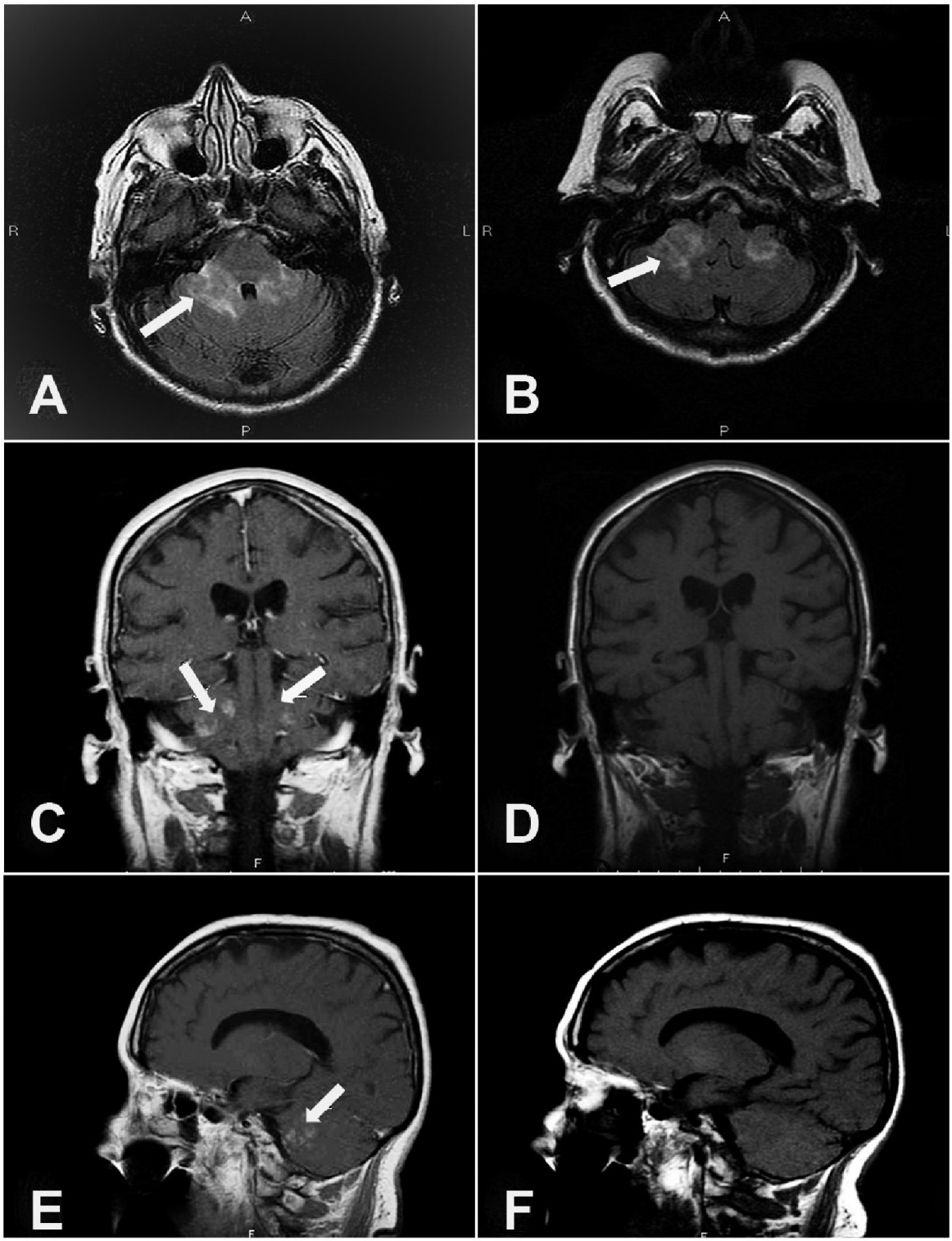

Fig. 1. Cranial MRI showing the cerebellar area of the AOAD patient at first hospital admission. **A.** A T2 axial FLAIR MRI shows bilateral, hyperintense lesions, particularly marked on the right side of the cerebellum and in the superior peduncle and dentate nucleus (arrows). **B.** A T2-weighted, axial FLAIR MRI of the caudal cranium shows heterogeneous and patchy lesions in both cerebellar peduncles, predominantly on the right side, thus, giving the impression of a mass effect. **C.** A T1-weighted, coronal MRI with contrast enhancement shows bilateral cerebellar lesions. **D.** The T1-weighted, coronal MRI without contrast enhancement does not reveal the cerebellar lesions. **E.** A T1-weighted, sagittal MRI with contrast enhancement reflects patchy cerebellar lesions. **F.** A T1-weighted, sagittal MRI shows apparent atrophy of the cortex with mild ventricular dilatation.

hyperintense lesions on both cerebellar lobules and peduncles, predominating on the right side in the white matter (Fig. 1A). Contrast enhancement revealed, in coronal and sagittal T1 images, irregular lesions in the cerebellum, which were not observable otherwise (Fig. 1B-F).

The first diagnostic conclusion was a pan-cerebellar syndrome of subacute, chronic evolution, suggesting a possible primary or inflammatory neoplastic process.

Six months later, the patient was readmitted to hospital after getting worse. Analyses verified high levels of antinuclear antibodies ANA, 1/160, auto-antibodies to the small molecular weight ribonucleo-proteins (positive anti-Ro/SS-A), an IgG level of 2364 mg/100mL, and an RF of 97.4 lU/mL, accompanied by lachrymal dryness, so that Sjögren syndrome was suspected.

New MRI confirmed persisting cerebellar alterations, while hyperintense lesions in the white brain matter, coinciding with the right, semioval centre, were identified in axial FLAIR sequences (Fig. 2A) together with lesions in the periventricular areas in T2 axial FLAIR sequences (Fig. 2B). Cranial MR angiography and continuous transcranial Doppler ultrasonography did not reveal any abnormalities. Osteoarthrosis of the hip was detected by simple X-ray diagnosis.

The patient consulted another hospital, where a suspicious-zone cerebellar biopsy, taken by means of MRI stereotaxy, resulted in a diagnosis of non-specific gliosis.

In the following five months, her symptomatology worsened. MRI in T2 axial FLAIR sequences showed hyperintense cerebellar lesions in the white and grey matter, covering peduncles, dentate nucleus, and vermis, with patches in the brainstem, pontine zone, and tegmentum (Fig. 3A-D).

The electroencephalogram (EEG) tracing was pathological with a pronounced diffuse disorganisation and had a baseline activity for the slow alpha and theta bands of 6-7 Hz with a mean amplitude of 40-50 uV. No beta activity was detected in frontal and posterior regions.

The ophthalmological examination revealed grade I hypertensive retinopathy with bilateral exophthalmus.

Finally, three months later, the patient was readmitted to hospital due to deterioration with a torpid evolution in her general condition and a lack of spontaneous movement in all four limbs, reduced consciousness, malnutrition, diarrhoea syndrome, bilateral pleural effusions, atelectasis and alveolar infiltrate in the left basal hemithorax, probably due to aspiration pneumonia, as diagnosed by thorax X-ray. Doppler ultrasound examination showed deep vein thrombosis in the left femoral vein. Fifteen months after her first hospital admission, the fatal evolution of the patient concluded with cardiac arrest and lethal exitus, 23 months after the first symptoms had become apparent.

Clinical autopsy

The most remarkable observations from gross pathology were a poor nutritional status, bilateral pleural effusion with condensed lungs, and no pleural adhesion. Left ventricular hypertrophy of the heart and marked arteriosclerosis in the thoracic aorta and abdominal and iliac arteries were observed. The two implanted stents were detected in the corresponding renal and femoral artery. The brain weighed 1248 g and conserved its circumvolutions. Abundant, cloudy cerebrospinal fluid contents in the posterior fossa, post-biopsy hygroma formation, as well as obvious thinning and atrophy of the upper cervical spinal cord were observed. The macroscopic impression of the cerebellum was atrophic and liquefied, like undergoing autolysis. The largely white aspect of the sections, particularly marked in the

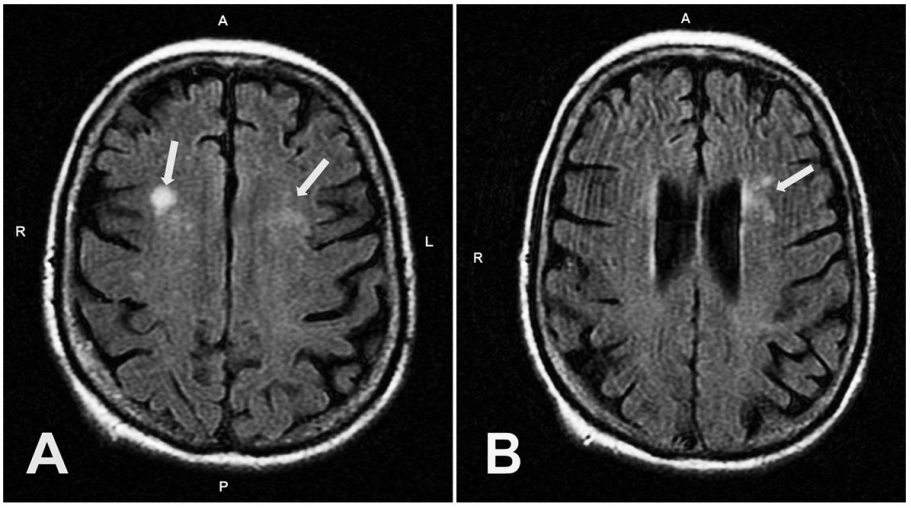

Fig. 2. MRI of the cerebral cortex. **A.** An axial FLAIR MRI shows lesions in the white matter, particularly a focal nodule that coincides with the right semioval centre. **B.** A T2 axial FLAIR MRI exhibits punctiform lesions at left lobule level in the periventricular area.

centre of the vermis, extended to the peduncles, the bulb, and the brainstem.

Histopathological and immunohistochemistry study

The alveolar pulmonary and bilateral bronchial areas held leukocyte infiltrates with abundant oedematous fluid, compatible with bronchopneumonia. The congested and fibrous meninges, especially in the right posterior fossa, coincided with a post-biopsy scarring or hygroma zone. Moderate atheromatosis was seen in the Willis polygon and basilar arteries. The histological

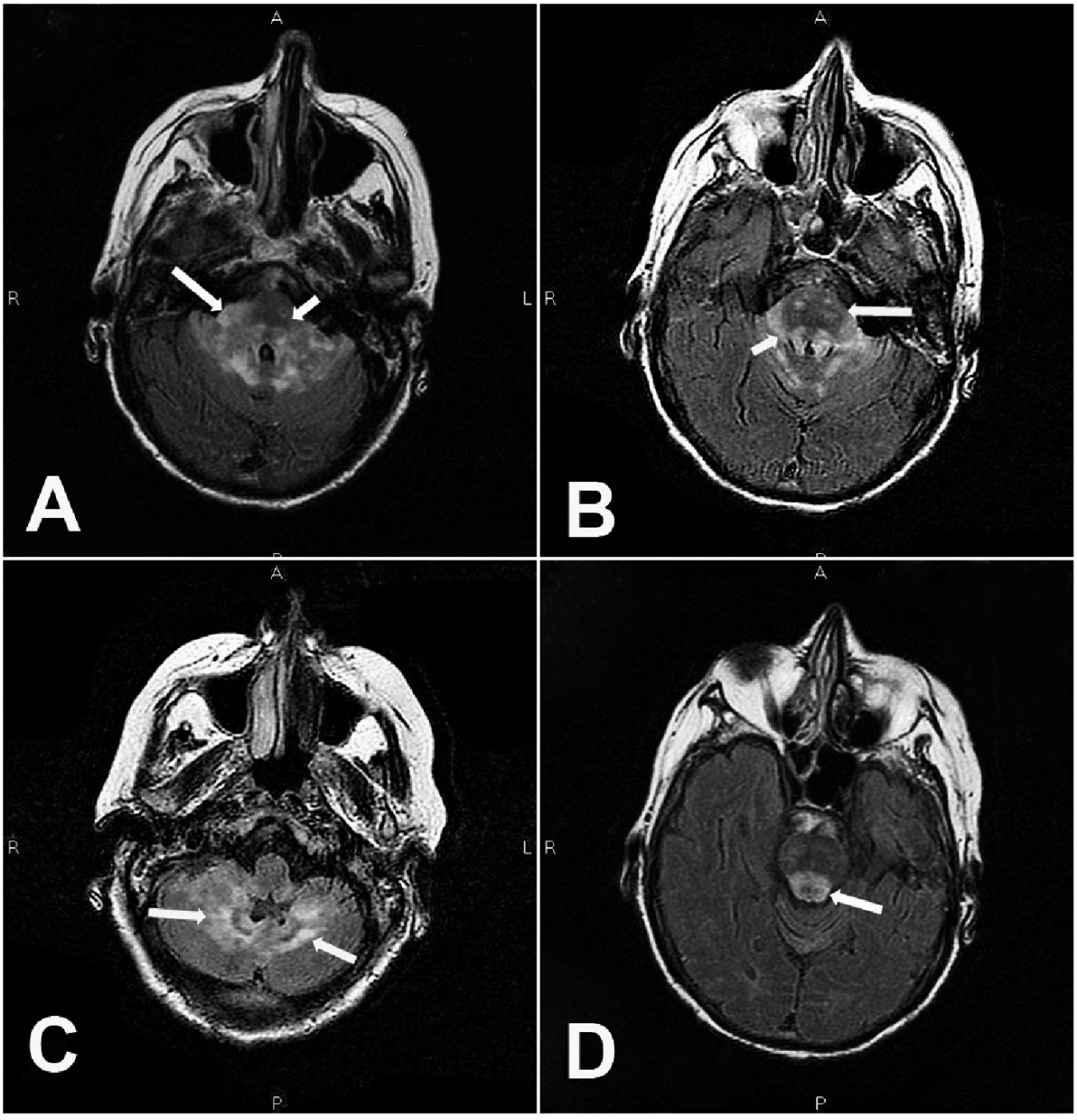

Fig. 3. T2 axial FLAIR MRI follow up of the cerebellar zone at late stage of the disease. **A.** Hyperintense lesions at bilateral cerebellar level with peduncle, brainstem, and tegmentum involvement. **B.** Patchy lesions in the pons and tegmentum areas are apparent. **C.** In cranio-caudal direction, cerebellar lesions near the orifice of the IV ventricle, which affect the vermis, are evident. **D.** Manifest lesions at medulla oblongata level.

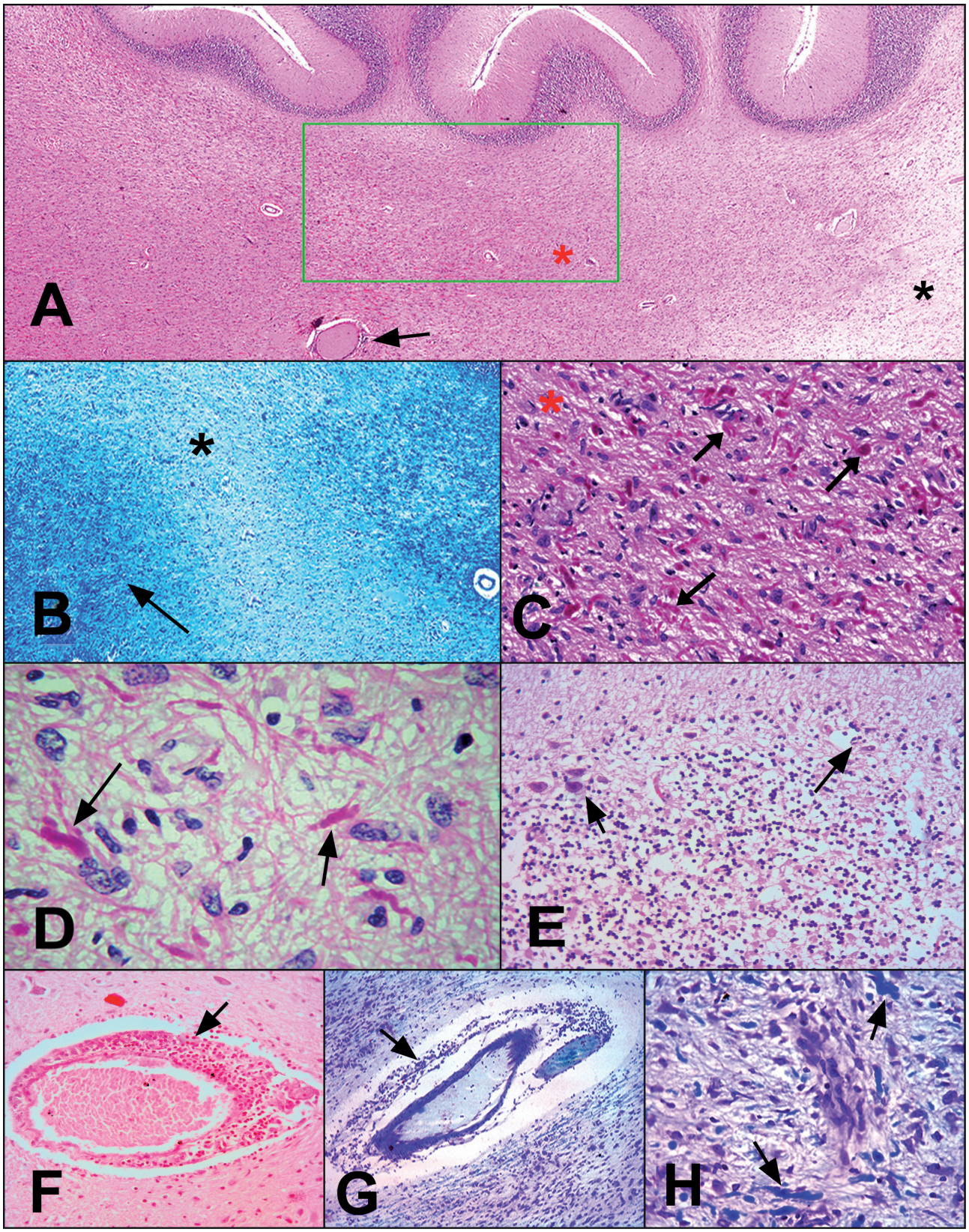

Fig. 4. Histopathological aspects of cerebellar involvement in AOAD. **A.** Overview of subcortical, cerebellar white matter with gliosis (boxed area, red star) and demyelination at the right edge (black star). A blood vessel with pericapillary lymphocyte infiltrates emerges at the bottom (arrow). H&E stain. **B.** Subcortical cerebellar white matter. Gliosis (arrow) and demyelinated area (star). Kluver-Barrera stain. **C.** Area of gliosis at higher magnification showing fibrous astrocytes and evenly distributed, numerous Rosenthal fibres (arrows). H&E stain. **D.** Cerebellar peduncle white matter with pleomorphic astrocytes and abundant Rosenthal fibres (arrows). H&E stain. **E.** Cortical cerebella grey matter. Damaged and atrophic Purkinje cells (arrows, from left to right). H&E stain. **F.** Subcortical cerebellar area and vermis. Capillaries with peripheral lymphocyte infiltrates. H&E stain. **G.** As F., but Kluver-Barrera stain. **H.** Gliotic, cerebellar area with Rosenthal fibres (arrows) stained for myelin. Kluver-Barrera stain. A, x 10; B, G, x 100; C, E, F, x 200; D, x 1000; H, x 400.

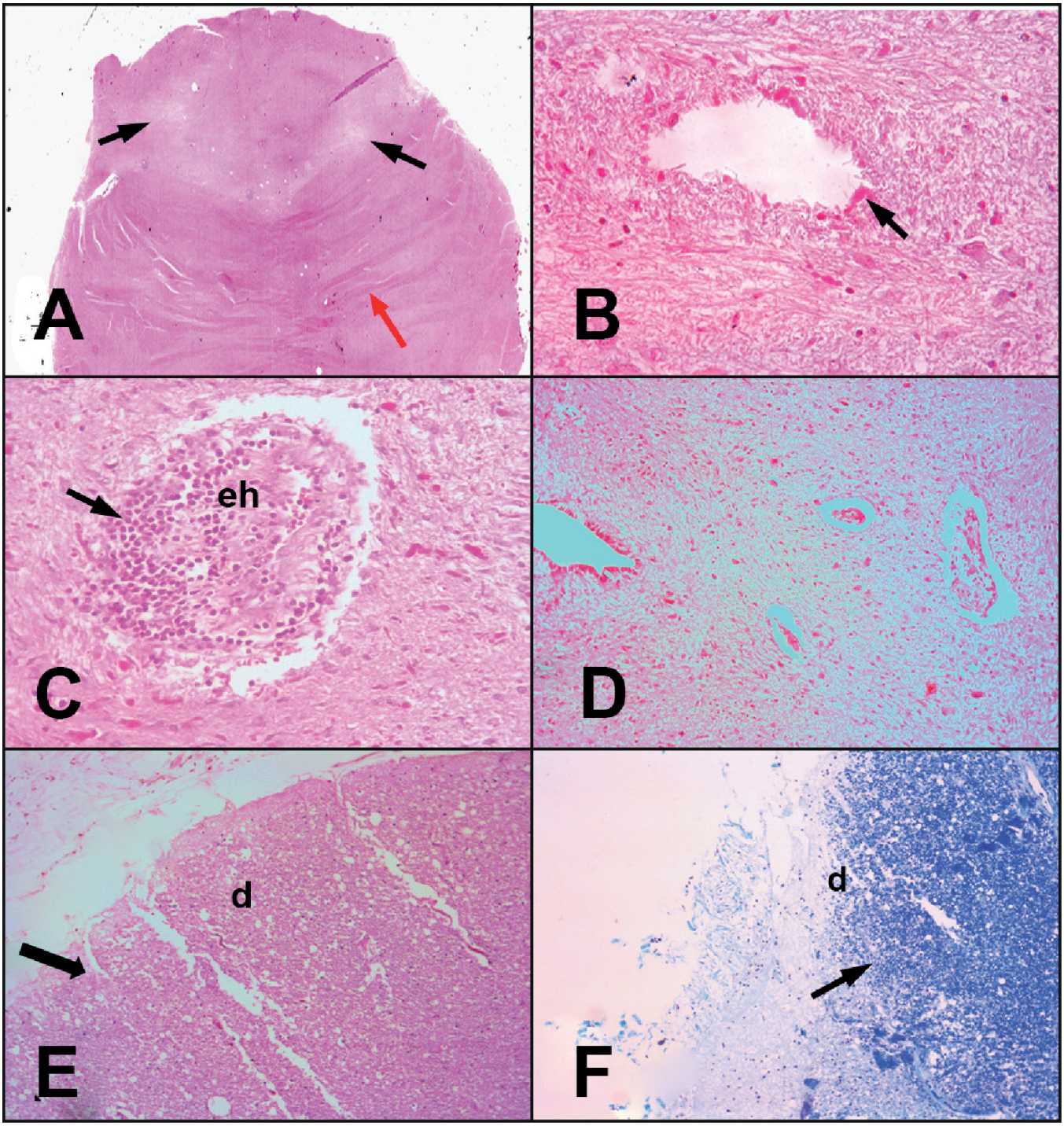

Fig. 5. Lesions of the brain stem, medulla oblongata, and spinal cord in AOAD. **A.** Brainstem at low magnification. Demyelinated zone in the tegmentum area (black arrows); pontine fibres (red arrow). H&E stain. **B.** Tegmentum area in the brainstem. Gliosis and perivascular Rosenthal fibres (arrow). H&E stain. **C.** Pontine area in the brainstem. Capillary with endothelial hyperplasia (eh), lymphocyte infiltrate (arrow), and a reduced lumen. Altered glia with Rosenthal fibres outside the capillary. H&E stain. **D.** Medulla oblongata. Demyelination with Rosenthal fibres. H&E stain. **E, F.** Spinal cord. Demyelinated subcortical areas (d, arrows). H&E and Kluver-Barrer stain, respectively. A, x 10; B, C, x 200; D-F, x 100.

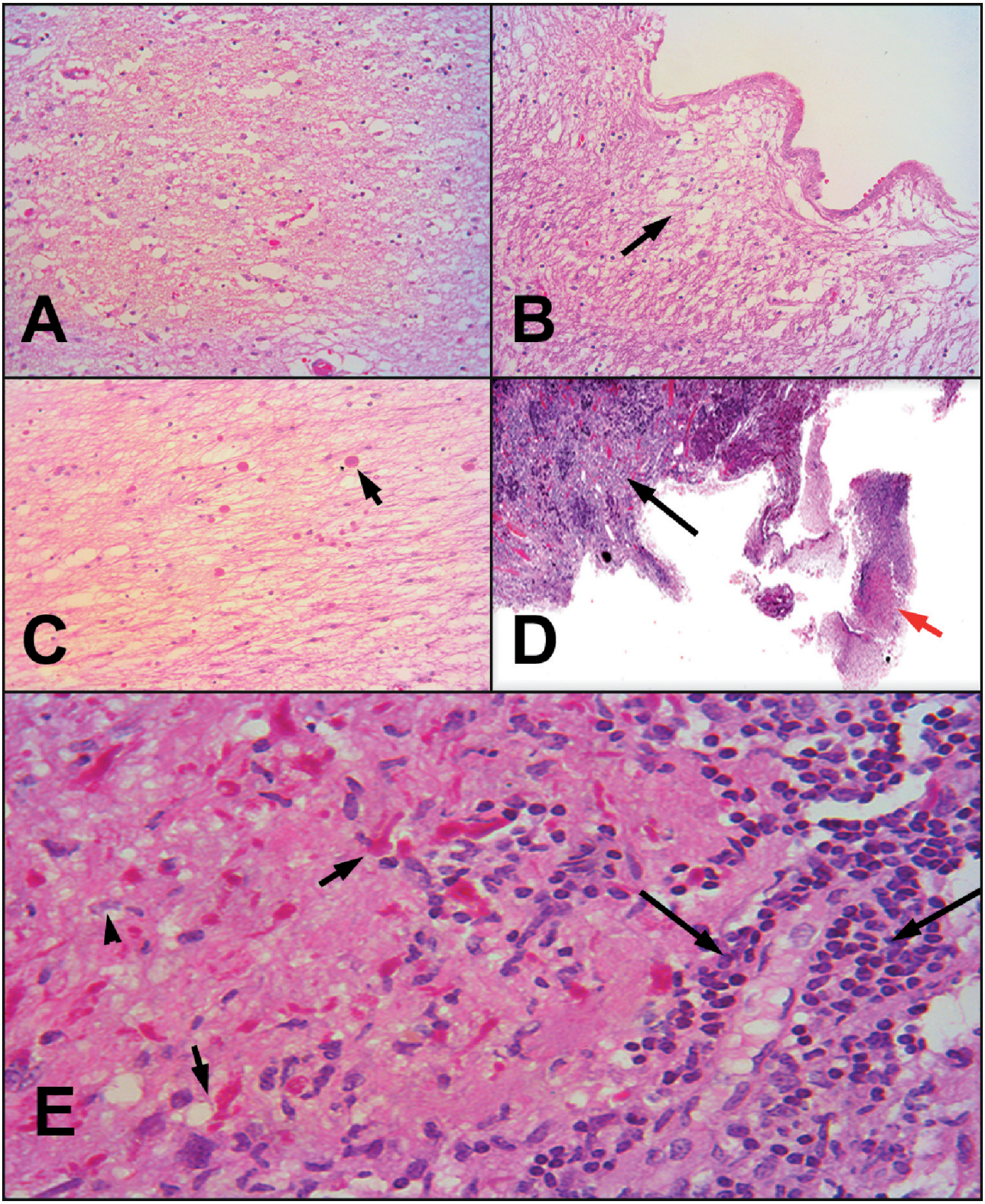

Fig. 6. Cerebral hemisphere lesions in AOAD. **A.** The white matter of the cerebral cortex in the right semioval centre shows demyelination and eosinophilic microfibres. H&E stain. **B.** Periventricular area with demyelination (arrow), H&E stain. **C.** Corpus callosum with gliosis, demyelination, and deposits compatible with amylaceous bodies (arrow). H&E stain. **D.** Detached pituitary fragment compatible with neurohypophysis. Adenohypophysis (black arrow), fragment (red arrow). H&E stain. **E.** The neurohypophysis-derived fragment shows pituicytes in a vacuolated area (arrow head), Rosenthal fibres (short arrow), and perivascular, lymphocyte infiltrates (long arrows). H&E stain. A-C, x 200; D, x 2; E, x 400.

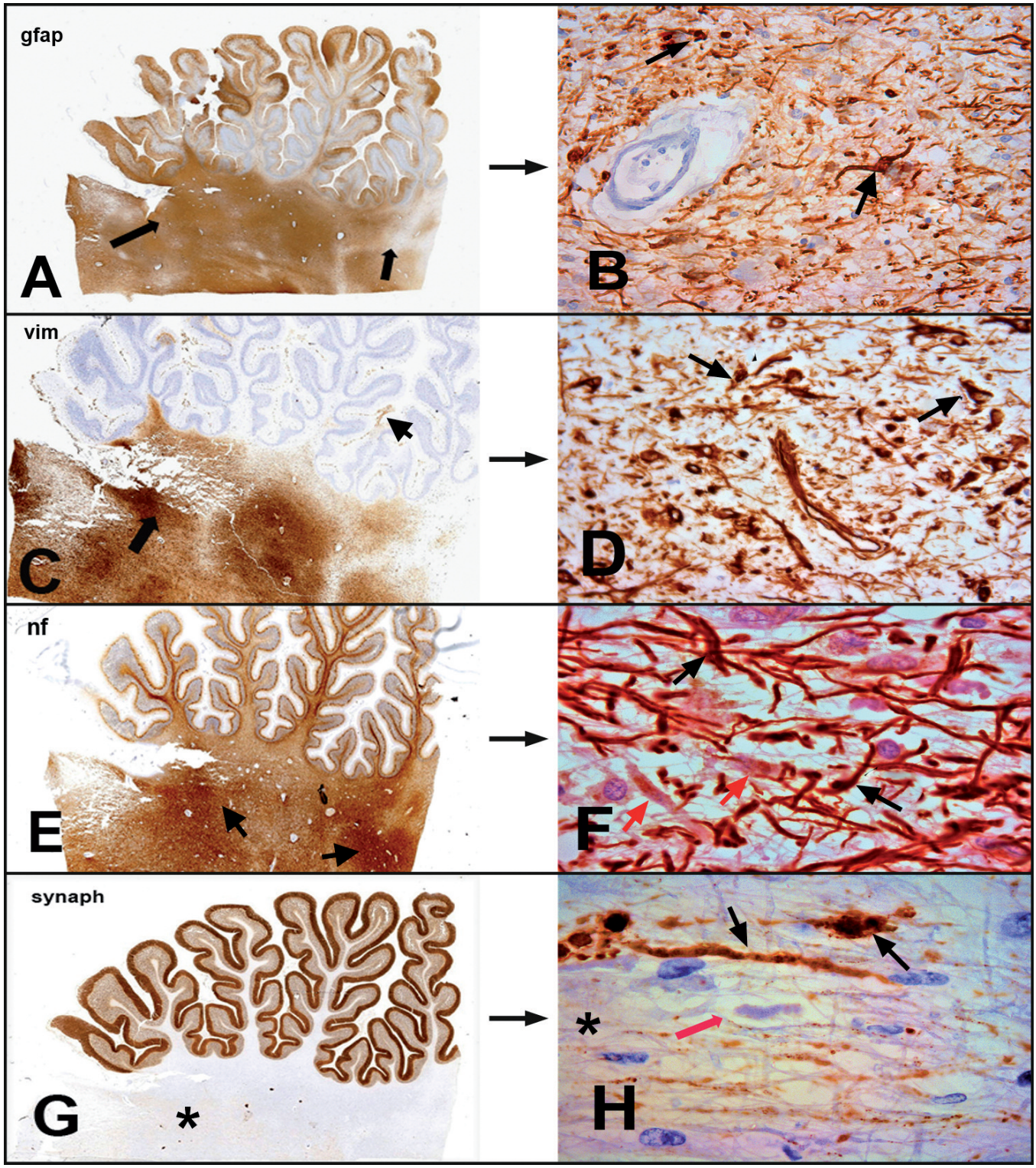

Fig. 7. Immunohistochemical staining of the cerebellum in AOAD. **A.** Overview showing strong staining for GFAP; a gliotic and demyelinated area (arrows). **B.** Positive staining for GFAP in glia and Rosenthal fibres (arrows). **C.** Overview showing strong staining for vimentin, particularly in the gliotic zone of the white matter (arrow), while in the grey matter only capillaries stained positive (short arrow). **D.** Strong staining for vimentin in glia, astrocytes, and Rosenthal fibres (arrows). **E.** Overview showing staining for neurofilament protein; stronger staining intensity is apparent in gliotic foci (arrows). **F.** Neurofilament protein staining at higher magnification. Apparently fragmented nerve fibres, forming crossings and thickenings. Irregular and thickened nervous filaments in between the glia (black arrows), while Rosenthal fibres did not stain (red arrows). **G.** Overview showing staining for synaptophysin in a synaptic area of the cerebellum. White matter with weak and diffuse immunostaining (star). **H.** Weak staining for synaptophysin, coarse and fragmented in axonal nerve fibres (arrows). Remarkable are the synaptophysin-negative glial components and Rosenthal fibres (red arrow). A, x 2; B, D, x 400; C, E, G, x 10; F, H, x 1000.

study of both parotid glands did not exhibit significant alterations.

In the white matter of the peduncles and dentate nucleus, in the subcortical zone of both cerebellar hemispheres, areas of gliosis alternated with clearer, demyelinated ones, containing fibrous and pleomorphic astrocytes and abundant, diffuse or perivascular arranged Rosenthal fibres of variable size, observable with H&E and Kluver-Barrera stain (Fig. 4A-E). Perivascular lymphocyte infiltrates were observed in the cerebellar subcortical zone and the vermis and upper layer of the cerebellar cortex, matching gliotic areas with Rosenthal fibres (Fig. 4F-H). In addition, Purkinje cell atrophy and degeneration was detected. (Fig. 4E).

Also, in the brainstem, tegmentum, and pontine zone, we found moderate gliosis with demyelination, Rosenthal fibres, and damaged neurons in the nuclei of the pons. A capillary exhibited lymphocytic infiltrates and endothelial hyperplastic thickening. The medulla oblongata showed demyelination and Rosenthal microfibrils, the bulbar olive displayed demyelination, and the upper spinal cord mild gliosis and demyelination as well (Fig. 5A-F).

Discrete gliosis was found in the frontal, parietal, and temporal areas of the cerebral white matter, while demyelination was detected in the right semioval centre, the periventricular areas, as well as the corpus callosum, where amylaceous bodies were observed. Finally, a fragment apparently originating from the neurohypophysis, with pituicytes, mild gliosis with Rosenthal fibres, in a vacuolated area and perivascular lymphocyte infiltrates attracted attention (Fig. 6A-E).

Immunohistochemical staining intensity against GFAP was strong in all the numerous hypertrophic fibres

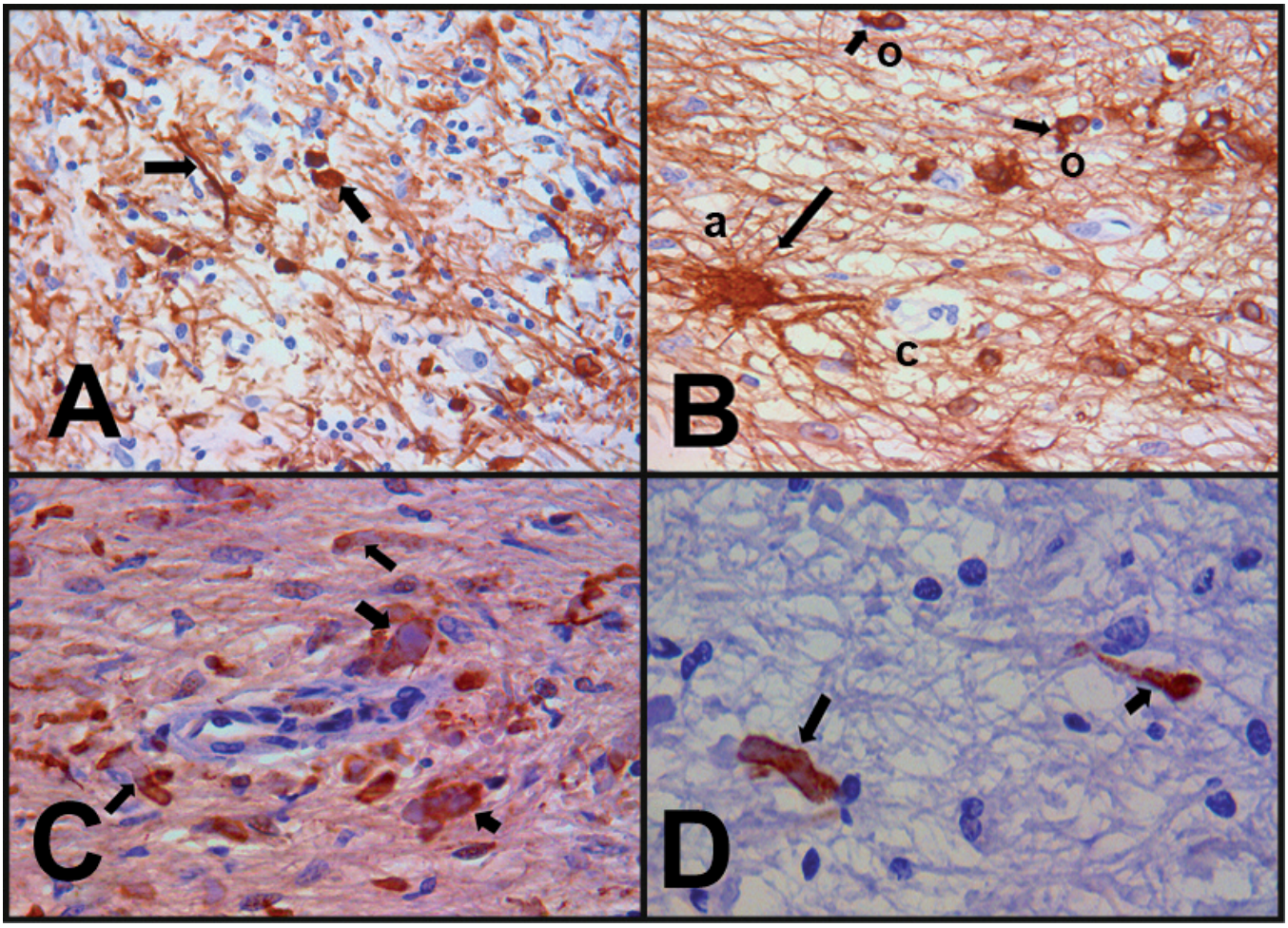

Fig. 8. Immunohistochemical staining for heat shock proteins in cerebellum. **A.** Strong staining for alpha B-crystallin in Rosenthal fibres and astrocytes. Positive staining in reactive astrocytes and gliosis (arrows). **B.** Positive staining for alpha B-crystallin (arrows) in astrocytes (a) near capillaries and in oligodendrocytes (o). **C.** Positive staining for ubiquitin in Rosenthal fibres, even stronger at the periphery. Remarkable is the cytoplasmic reactivity within the astrocytes (arrows). **D.** Positive staining for hsp 27, tending to precipitate at the periphery of sporadic, dispersed Rosenthal fibres (arrow). x 400.

in the white matter, particularly in gliotic and demyelinated zones and Rosenthal fibres, even stronger in thick fibres, as well as in the cytoplasm of astrocytes. The latter were enlarged with several active, radial extensions, granular cytoplasm, and large nuclei, creating an image of polymorphism. (Fig. 7A-B). In gliotic areas, strong vimentin labelling of Rosenthal fibres as well as cytoplasm of astrocytes was observed, whereas demyelinated areas had lost antibody reactivity (Fig. 7A-D).

Intense immunoreactions against neurofilament protein was found in the gliotic areas, where it formed a discrete, thickened and fragmented pattern, which alternated with or was found in proximity to the Rosenthal fibres, without forming part of them, and to the altered glia (Fig. 7E-F). On the other hand, intense synaptophysin labelling was detected in the cerebellar grey matter and cortex, while there was little, coarse and fragmented staining in the areas of reactive gliosis (Fig. 7G,H).

Finally, the anti-alpha B-crystallin antibody strongly labelled Rosenthal fibres as well as the altered glia and astrocyte somata. The anti-ubiquitin antibody deposited in Rosenthal fibres and tended to arrange in peripheral lumps, while the stress protein anti-hsp27 antibody only sporadically labelled Rosenthal fibres and generated irregular and peripheral patterns (Fig. 8A-D).

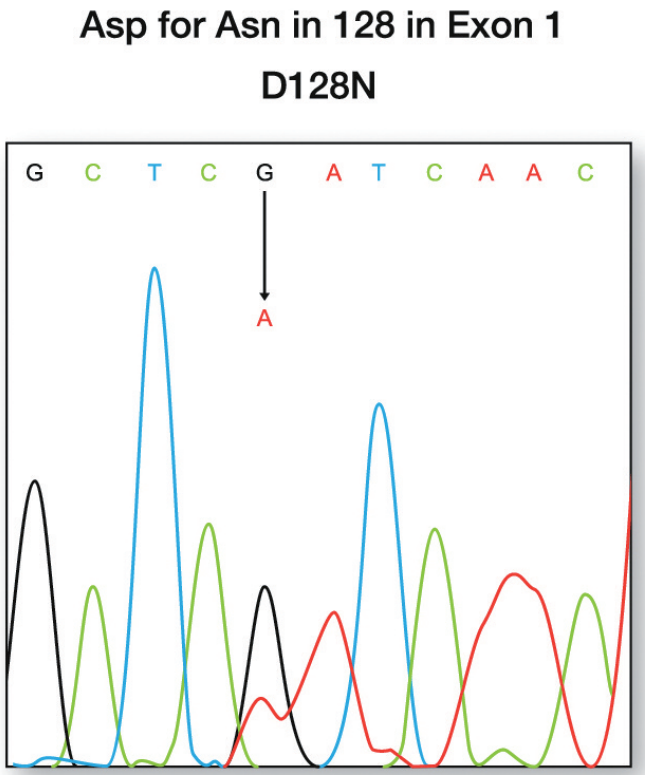

Fig. 9. DNA sequence of GFAP exon 1. A G382-to-A transversion produced an ASP 128 to ASN substitution in exon 1.

Molecular study

Direct sequencing of the GFAP gene uncovered a heterozygous point substitution, i.e. a G to A transversion at nucleotide 382, which resulted in an ASP 128 to ASN substitution in exon 1. We did not find this mutation in DNA from healthy subjects (Fig. 9).

Discussion

Clinical data

Here, we present a case of insidious AOAD that manifested as a cerebellar syndrome with fatal evolution. A diagnosis was only possible at autopsy, as neither clinical nor MRI data was satisfactory.

Comparing disease progression and clinical symptoms of the patient with the first MRI, we observed that intense bilateral lesions of the white matter of the cerebellum, peduncles, dentate nucleus, and vermis corresponded with symptoms such as ataxic gait, language alterations, tremor, and nystagmus without loss of strength in the extremities and with preserved muscle reflexes. No cognitive changes were observed, consistent with MRI-undetectable abnormalities in the cerebrum, encephalon trunk, and medulla oblongata.

At the two following hospital admissions, after six and again after five additional months of evolution, the cerebellar lesions were accentuated and new ones had appeared in the cerebral white matter, right semioval centre, and periventricular area. Later on, lesions of moderate intensity were detected in the brainstem, base, medulla oblongata, and in the form of patches in the tegmentum and pons, coinciding with the worsening of the patient. Altogether, this MRI pattern of lesions had been described as typical in AOAD (Brenner et al., 2001; Farina et al., 2008; Pareyson et al., 2008; Prust et al., 2011).

In the final phase of the disease, during the last three months, worsening was very noticeable and progressive with a complete lack of movement in all four limbs, reflecting involvement of the brainstem–spinal cord junction, and with pyramidal signs, all that affecting the patient's consciousness until a bronchopneumonia led to her exitus.

A drawback of the present work is that no MRI analyses of the descending spinal cord were performed. However, at autopsy, we were able to detect macroscopic signs of alteration and atrophy of the proximal spinal cord, though it was not possible to study the entire medulla.

Therefore, we present a case that matches the characteristics of AOAD type II in accordance with Prust et al. (2011), with manifestations related to the brainstem, bulbar and spinal cord junction, and predominance in the posterior fossa, which started in the

cerebellum with ataxia and cerebellar syndrome and subsequently extended to the brainstem, bulbar and spinal cord.

MRI reflected lesions with atrophy in these zones as well as supratentorial areas, also described by Pareyson et al. (2008) and Farina et al. (2008). The comparison between clinical and MRI data allowed to follow the evolution of the disease in detail and corroborate it by autopsy.

Histopathological and immunohistochemistry evaluation-Rosenthal fibres

The final, histopathological findings revealed involvement of the cerebellar white matter with alternating changes of reactive gliosis and demyelination, accompanied by abundant Rosenthal fibres and occasional, pericapillary lymphocyte infiltrates, especially in the vermis. In addition, hypertrophic astrocytes, damaged neurons, loss of Purkinje cells, and an overall pattern of leukodystrophy characterised the areas, which were the initially most damaged and the hyperintense ones in MRI.

However, in the brainstem, pons and tegmentum, medulla oblongata, bulbar olive, and upper spinal cord signs were attenuated; there was only gliosis, demyelination, and a few Rosenthal fibres. Lesions with demyelination and gliosis in the cerebral white matter of the supratentorial region coincided with the MRI of the right semioval centre and periventricular zones.

Published work attributes these signs, such as altered astrocytes, demyelination, and the presence of Rosenthal fibres to type II AD, less accentuated than type I and extending over a longer time span. The occurrence of these lesions, their evolution, and the preponderance of the mentioned territories in the CNS are not clear yet (Sosunov et al., 2018).

Our data confirmed hypertrophy and hyperplasia of the gliosis-organising, fibrillary astrocytes and their prolongations, which coincided with areas of hyperintense MRI signals and very strong immunohistochemical staining for GFAP. In a severe and chronic process such as AD, with reactive gliosis, marked astrocyte hyperactivity and hypertrophy, including Rosenthal fibre formation, this ability of the astrocytes may be increased and may contribute to or even be the cause of a neurodegenerative process in this disease (Guillamón-Vivancos et al., 2015; Messing, 2018; Sosunov et al., 2018).

Hence, if we compare clinical symptoms, MRI, and histopathology data, we could hypothesise that in this case of AOAD the oldest lesions are the classically described ones of altered gliosis and Rosenthal fibre formation, and demyelination is a subsequent occurrence.

According to various authors, histologically observable Rosenthal fibres are the hallmark to diagnose AD (Iwaki et al., 1993; Wippold et al., 2006; Quinlan et al., 2007; Pareyson et al., 2008). Nonetheless, they are not pathognomonic, as they can also appear in cerebral scars and pilocytic astrocytomas. However, Rosenthal fibres obviously participate, in association with fibrous astrocytes, in AD pathogenesis.

When observed by light microscopy, Rosenthal fibres are habitually described as round or elongated hyaline bodies. We detected variably sized, eosinophilic deposits, cylindrical and granular particles, and glial filaments upon H&E staining. Immunohistochemical labelling revealed abundant GFAP protein and the heat shock proteins alpha B-crystallin, ubiquitin, and hsp27, all in a context of aggregation and signs of cell stress, probably due to protein misfolding, as described in AOAD and in murine models (Iwaki et al., 1993; Hagemann et al., 2006; Sawaishi, 2009; Wang et al., 2011; Yoshida and Nakagawa, 2012; Heaven et al., 2016; Sosunov et al., 2017, 2018).

We have detected ubiquitin at sites with high Rosenthal fibre density and lumps at the periphery, which agrees with the literature stating that the ubiquitin proteosome participates in the accumulation of the cellular stress proteins alpha B-crystallin and hsp27 (Quinlan et al., 2007). We observed intense alpha B-crystallin labelling in Rosenthal fibres, glia, cytoplasm of astrocytes and their extensions, while scarce clusters of hsp27 tended to form at the periphery, similar to ubiquitin.

We cannot provide a solid explanation for how to interpret this morphological phenomenon in Rosenthal fibre formation. However, we hypothesise that those fibres were already stable, in a final phase of aggregation, as they were detected in histological sections of the cerebellum. On the other hand, they may no longer have induced ubiquitination of the misfolded proteins at that stage, whereas alpha B-crystallin activity may still have continued.

In experimental models, Rosenthal fibres formed upon overexpression of wild type GFAP with scarce hsp27 and a lack of alpha B-crystallin, but not in the presence of mutant GFAP (Bachetti et al., 2010). However, the proteomic approach of Heaven et al. (2016) does not support these differences, as heat shock protein levels were low under both conditions. Our observations indicated high levels of alpha B-crystallin and ubiquitin and very low levels of hsp27.

We also found immunostaining against vimentin associated with Rosenthal fibres, particularly in gliotic areas of the white matter. A GFAP mutation, namely R239C, has been described to interfere both *in vitro* and in transient cell transfection experiments in the assembly of this protein. Vimentin has been related to gliosis as a co-polymer of the mutated GFAP, engaging in its solubility and the assembly of intermediate filaments and proteins in intra- and intermolecular cross-links (Hsiao et al., 2005). Protein enrichment studies have described vimentin as a part of Rosenthal fibres in mice and human (Heaven et al., 2016), which most likely was

also the reason for our observation.

Neuronal alteration and loss in AD. Neurofilament and synaptophysin

Another topic to be taken into account is the potential influence of leukodystrophy on the rest of the cell populations in AD, such as neurons in the cerebellum and encephalon. In line with other authors (Chang et al., 2015), our light microscopy observations revealed a neuronal depopulation in some of the changed areas as well as a alteration and loss of Purkinje cells.

Neuronal loss has been described in AD, though not as a relevant point. However, more attention is being paid to this phenomenon recently (Sosunov et al., 2018), such that, e.g., a Drosophila model for AxD has revealed neuronal loss due to glutamate toxicity (Wang et al., 2011).

Also, in mice with mutation-independent, abundant GFAP and Rosenthal fibres, gene expression levels of vesicular trafficking proteins, like synaptophysin, neurofilament, and others are decreased, suggesting loss of neurons, synapses, or a developmental or functional defect (Hageman et al., 2005).

Little is known about neurofilament and synaptophysin in axons of the white matter in AD. To detect neurofilament protein in reactive gliosis, we used an antibody that recognises a 70 kD phosphorylated form of the neurofilament triple protein (Liem and Messing, 2009). Reactivity to this antibody is normally found in the cytoplasm of neurons and their processes, but not in astrocytes.

We have observed intense neurofilament protein labelling in gliosis, which was less pronounced in demyelinated zones, thereby detecting some fragmentation and neurofilament thickenings alternating with Rosenthal fibres, but apparently no contribution to their formation. In this regard, Chang et al. (2015) found, using the same technique, axonal preservation and certain accumulations or axonal swellings that would indicate damage.

Labelling of the membrane protein synaptophysin visualised coarse and fragmented axonal extensions in the zones of reactive gliosis. This protein has been described as a marker of axonal damage in experimental demyelinating and neuroinflammatory lesions caused, e.g., by cuprizone toxicity or an infection model of demyelination, the Theiler's murine encephalomyelitis virus (TMEV). In addition, synaptophysin labelling was applied to analyse the CNS of patients with multiple sclerosis (MS). It matched with reactive microglia in the late phase of demyelination and resembled spheroids or bulbs, which, if persistent, would indicate axonal damage (Gudi et al., 2017). We detected labelled, elongated synaptophysin deposits, which looked like residual material without any signs of inflammation, though, in the case of MS, these deposits appear in inflammatory regions. One might reasonably conclude that the occurrence of synaptophysin is a common sign of MS and AOAD. In this context, additional, more accurate studies are needed in human AD.

Perivascular lymphocyte infiltration and ANA

Lymphocyte infiltrates were detected in capillaries of the cerebellum, particularly in the vermis, the brainstem, as well as a fragment of the neurohypophysis, matching with altered glial zones with Rosenthal fibres. A blood vessel of the brainstem exhibited parietal, hyperplastic thickening without any other sign of alteration, so that we could not find any explanation for it. However, there is very little known on whether AOAD is an inflammation-based disease.

Lymphocyte infiltration has already been described in human as well as murine models, where AxD mice show a significant upregulation of a number of inflammatory genes (Hagemann et al., 2005) with a pronounced immune response and marked microglial activation (Olabarria et al., 2015; Sosunov et al., 2018).

Moreover, Olabarria et al. (2015) described inflammatory signs in an autopsy-based report on two cases of children with type I AD, with T lymphocytes (CD3 +) around capillaries of the meninges, cerebral parenchyma, and the spinal cord. Although, the authors did not show data on lymphocytic B cells, this would be an interesting field of further research in this type of human AD.

In our case, ANA antibodies, accompanied by dry eye symptoms, were detected, so that Sjögren's syndrome was suspected but not confirmed on autopsy through altered parotid glands. The occurrence of Sjögren's syndrome has been recognised in other diseases, such as MS. The clinical presentation of the latter also comprises tremor, deterioration of motor function, and ataxia, depending on the severity of sclerosis in the cerebellum or other areas, which may physically and cognitively destroy the patient. In MS, the cerebellar and peduncle damages do not exhibit Rosenthal fibres but consist of demyelinating plaques, accompanied by macrophages, remnants of glial fibres, and perivascular inflammatory infiltrates, which contribute to neuronal death (Popescu et al., 2013; Huang et al., 2017; Izadi and Khosniat, 2017). Conversely, although no comparative analyses in T1 and T2 were performed, our MRIs with and without Gadolinium contrast did not verify vascular or inflammatory changes, a fact that would have indicated MS. These findings were subsequently confirmed by autopsy.

Despite a positive salivary gland scintigraphy, the above mentioned dry eye syndrome, RF factor, and ANA data no inflammation of the parotid gland at autopsy, nor Hashimoto's thyroiditis or any sign of hepatitis confirmed Sjögren's syndrome. However, we did discover vasculitis and autoimmune positive blood results in the present case. Therefore, we think that more evidence is needed to clarify whether AD may be an autoimmune disease.

The (c.382 G>A, p. D128N) mutation

Our molecular study detected the mentioned heterozygous missense mutation, previously reported in three cases of sporadic AOAD (Pareyson et al., 2008; Chang et al., 2015; Lee et al., 2017). All three have in common that the patients' age ranged from 52 to 68 years. Disease onset had been from months to 3 years before exitus, relatively short compared to other published cases, where the onset varied between 13 and 22 years prior to exitus (Li et al., 2005).

Clinical signs were disparate. Ataxia, e.g., the dominant and syndromal sign in our case, together with dysarthria, dysphagia, and nystagmus were only presented in the case of Lee et al. (2017), as Pareyson et al. (2008) solely reported gait abnormalities and Chang et al. (2015) initial paraplegia.

The MRI signs were the most consistent in the four cases and comprised the mostly detected cerebellar, bulbar, and upper spinal cord atrophy, as well as hyperintense lesions in cerebellum and brainstem. The histopathological study by Chang et al. (2015) and the here presented one, both from autopsies, showed the classic Rosenthal fibre and demyelination pattern in cerebellum, supratentorial region, corpus callosum, brainstem, and pons, while the remaining two studies did not provide morphological data.

Therefore, the cases, including this one, with the D128N mutation in the GFAP gene, correspond to a form of AOAD with lower brainstem involvement and affected spinal cord and posterior pyramidal tract as the most striking signs. The most noticeable sign in the here presented case was clearly the involved cerebellum.

As to the patient's final evolution, dysphagia is common in AOAD and requires special care, as is the case with dyspnoea. Given the final situation of disability, aspiration pneumonia was considered the cause of death and in fact, together with the other, secondary respiratory infectious processes, like bronchopneumonia, eventually led to the patient's death.

The four patients with the c.382 G>A (p.D128N) mutation displayed clinical characteristics of AOAD, although their symptoms were not alike. To our knowledge, this mutation has not been described in type I AD so far.

In conclusion, the c.382 G>A (p. D128N) mutation seems to condition a particular form of sporadic AOAD with characteristic clinical symptoms and MRI signs. The most characteristic initial feature, on clinical as well as MRI evaluation, was the cerebellar involvement. Rosenthal fibres, being key to a histopathological diagnosis, were detected in the cerebellum and brainstem, though only at autopsy. The occurrence of perivascular lymphocyte infiltrates and ANA antibodies should give rise to more in-depth studies of the disease background. Finally, the provided histological evidence that neurofilaments and synaptophysin were affected may contribute to better understand the pathogenesis of AD.

Acknowledgements. The authors would like to thank Dr. Martina K. Pec for translation and revision of the manuscript, Dr. Rafael Amador Trujillo and Dr. Guiomar Pinar Sedeño (Neurology Service of the Hospital Insular de Las Palmas de Gran Canaria) for the clinical information, and Dr. Teresa Ribalta Farres (Pathological Anatomy Service of the Hospital Clinic of Barcelona) for her diagnostic support. The authors also acknowledge David Cabrera and Alexis Alemán for iconographic and design support.

Conflict of interest. The authors have no conflict of interest to declare.

References

Alexander W.S. (1949). Progressive fibrinoid degeneration of fibrillary astrocytes associated with mental retardation in a hydrocephalic infant. Brain J. Neurol. 72, 373-381.

Bachetti T., Di Zanni E., Balbi P., Bocca P., Prigione I. and Deiana GA. (2010). In vitro treatments with ceftriaxone promote elimination of mutant glial fibrillary acidic protein and transcription down-regulation. Exp. Cell Res. 316, 2152-2165.

Brenner M., Johnson A.B., Boespflug-Tanguy O., Rodriguez D., Goldman J.E. and Messing A. (2001). Mutations in GFAP, encoding glial fibrillary acidic protein, are associated with Alexander disease. Nat. Genet. 27, 117-120.

Chang K-E., Pratt D., Mishra B.B., Edwards N., Hallett M. and Ray-Chaudhury A. (2015). Type II (adult onset) Alexander disease in a paraplegic male with a rare D128N mutation in the GFAP gene. Clin. Neuropathol. 34, 298-302.

Farina L., Pareyson D., Minati L., Ceccherini I., Chiapparini L and Romano S. (2008). Can MR Imaging Diagnose Adult-Onset Alexander Disease? Am. J. Neuroradiol. 29, 1190-1196.

Gudi V., Gai L., Herder V., Tejedor L.S., Kipp M., Amor S. Sühs K.W., Hansmann F., Beineke A., Baumgärtner W., Stangel M. and Skripuletz T. (2017). Synaptophysin is a reliable marker for axonal damage. J. Neuropathol. Exp. Neurol. 76, 109-125.

Guillamón-Vivancos T., Gómez-Pinedo U. and Matías-Guiu J. (2015). Astrocytes in neurodegenerative diseases (I): function and molecular description. Neurologia 30,119-129.

Hagemann T.L., Gaeta S.A., Smith M.A., Johnson D.A., Johnson J.A and Messing A. (2005). Gene expression analysis in mice with elevated glial fibrillary acidic protein and Rosenthal fibers reveals a stress response followed by glial activation and neuronal dysfunction. Hum. Mol. Genet. 14, 2443-2458.

Hagemann T.L., Connor J.X. and Messing A. (2006). Alexander disease-associated glial fibrillary acidic protein mutations in mice induce Rosenthal fiber formation and a white matter stress response. J. Neurosci. 26, 11162-11173.

Heaven M.R., Flint D., Randall S.M., Sosunov A.A., Wilson L., Barnes S., Goldman J.E., Muddiman D.C. and Brenner M. (2016). Composition of Rosenthal fibers, the protein aggregate hallmark of Alexander disease. J. Proteome Res.15, 2265-2282.

Hsiao V.C., Tian R., Long H., Der Perng M., Brenner M., Quinlan R.A. and Goldman J.E. (2005). Alexander-disease mutation of GFAP causes filament disorganization and decreased solubility of GFAP. J. Cell Sci. 18, 2057-2065.

Huang W.J., Chen W. and Zhang X. (2017). Multiple sclerosis: Pathology, diagnosis and treatments. Exp. Ther. Med. 13, 3163-3166.

Iwaki T., Iwaki A., Tateishi J., Sakaki Y. and Goldman J.E. (1993). Alpha B-crystallin and 27-kd heat shock protein are regulated by stress conditions in the central nervous system and accumulate in Rosenthal fibers. Am. J. Pathol. 143, 487-495.

Izadi S. and Khoshniat S. (2017). Evaluation of serum auto antibodies in multiple sclerosis patients: A case control study. Int. Clin. Neurosc. J. 4, 25-28.

Lee S-H., Nam T-S., Kim K-H., Kim J.H., Yoon W., Heo S-H., Kim M.J., Shin B.A., Perng M.D., Choy H.E., Jo J., Kim M.K. and Choi S.Y. (2017). Aggregation-prone GFAP mutation in Alexander disease validated using a zebrafish model. BMC Neurol. 7,17, 175.

Li R., Messing A., Goldman J.E. and Brenner M. (2002). GFAP mutations in Alexander disease. Int. J. Dev. Neurosci. 20, 259-268.

Li R., Johnson A.B., Salomons G., Goldman J.E., Naidu S., Quinlan R., Cree B., Ruyle S.Z., Banwell B., D'Hooghe M., Siebert J.R., Rolf C.M., Cox H., Reddy A., Gutiérrez-Solana L.G., Collins A., Weller R.O., Messing A., van der Knaap M.S. and Brenner M. (2005). Glial fibrillary acidic protein mutations in infantile, juvenile, and adult forms of Alexander disease. Ann. Neurol. 57, 310-326.

Liem R.K.H. and Messing A. (2009). Dysfunctions of neuronal and glial intermediate filaments in disease. J. Clin. Invest.119,1814-1824.

Messing A. (2018). Alexander disease. Handb Clin. Neurol.148, 693-700.

Messing A., Goldman J.E., Johnson A.B. and Brenner M. (2001). Alexander disease: new insights from genetics. J. Neuropathol. Exp. Neurol. 60, 563-573.

Namekawa M., Takiyama Y., Honda J., Shimazaki H., Sakoe K. and Nakano I. (2010). Adult-onset Alexander disease with typical 'tadpole' brainstem atrophy and unusual bilateral basal ganglia involvement: a case report and review of the literature. BMC Neurol. 10, 21.

Olabarria M., Putilina M., Riemer E.C. and Goldman J.E. (2015). Astrocyte pathology in Alexander disease causes a marked inflammatory environment. Acta Neuropathol. (Berl). 130, 469-486.

Pareyson D., Fancellu R., Mariotti C., Romano S., Salmaggi A., Carella F., Girotti F., Gattellaro G., Carriero M.R., Farina L., Ceccherini I. and Savoiardo M. (2008). Adult-onset Alexander disease: a series of eleven unrelated cases with review of the literature. Brain J. Neurol.131, 2321-2331.

Pekny T., Faiz M., Wilhelmsson U., Curtis M.A., Matej R., Skalli O Pekny M. (2014). Synemin is expressed in reactive astrocytes and Rosenthal fibers in Alexander disease. APMIS Acta Pathol. Microbiol. Immunol. Scand.122, 76-80.

Pixley S.K. and Vellis J. (1984). Transition between immature radial glia and mature astrocytes studied with a monoclonal antibody to vimentin. Brain Res. 317, 201-209.

Popescu B., Pirko I. and Lucchinetti C.F. (2013). Pathology of multiple sclerosis: where do we stand? Contin Minneap. Minn.19, 901-921.

Prust M., Wang J., Morizono H., Messing A., Brenner M., Gordon E., Hartka T., Sokohl A., Schiffmann R., Gordish-Dressman H., Albin R., Amartino H., Brockman K., Dinopoulos A., Dotti M.T., Fain D., Fernandez R., Ferreira J., Fleming J., Gill D., Griebel M., Heilstedt H., Kaplan P., Lewis D., Nakagawa M., Pedersen R., Reddy A., Sawaishi Y., Schneider M., Sherr E., Takiyama Y., Wakabayashi K., Gorospe J.R. and Vanderver A. (2011). GFAP mutations, age at onset, and clinical subtypes in Alexander disease. Neurology 77, 1287-1294.

Quinlan R.A., Brenner M., Goldman J.E. and Messing A. (2007). GFAP and its role in Alexander disease. Exp. Cell Res. 313, 2077-2087.

Reeves S.A., Helman L.J., Allison A. and Israel M.A. (1989). Molecular cloning and primary structure of human glial fibrillary acidic protein. Proc. Natl. Acad. Sci. USA 86, 5178-5182.

Sawaishi Y. (2009). Review of Alexander disease: Beyond the classical concept of leukodystrophy. Brain Dev. 31, 493-498.

Sosunov A.A., McKhann G.M. and Goldman J.E. (2017). The origin of Rosenthal fibers and their contributions to astrocyte pathology in Alexander disease. Acta Neuropathol. Commun. 5, 27.

Sosunov A., Olabarria M. and Goldman J.E. (2018). Alexander disease: an astrocytopathy that produces a leukodystrophy. Brain Pathol. Zurich Switz. 28, 388-398.

Sugiyama A., Sawai S., Ito S., Mukai H., Beppu M., Yoshida T. and Kuwabara S. (2015). Incidental diagnosis of an asymptomatic adult-onset Alexander disease by brain magnetic resonance imaging for preoperative evaluation. J. Neurol. Sci. 354, 131-132.

van der Knaap M.S., Naidu S., Breiter S.N., Blaser S., Stroink H., Springer S., Begeer J.C., van Coster R., Barth P.G., Thomas N.H., Valk J. and Powers J.M. (2001). Alexander disease: diagnosis with MR imaging. AJNR Am. J. Neuroradiol. 22, 541-552.

Wang L., Colodner K.J. and Feany M.B. (2011). Protein misfolding and oxidative stress promote glial-mediated neurodegeneration in an Alexander disease model. J. Neurosci. 31, 2868-2877.

Wippold F.J., Perry A. and Lennerz J. (2006). Neuropathology for the neuroradiologist: Rosenthal fibers. Am. J. Neuroradiol. 27, 958-961.

Yoshida T. and Nakagawa M. (2012). Clinical aspects and pathology of Alexander disease, and morphological and functional alteration of astrocytes induced by GFAP mutation. Neuropathology 32, 440-446.

Yoshida T., Sasaki M., Yoshida M., Namekawa M., Okamoto Y., Tsujino S., Sasayama H., Mizuta I., Nakagawa M. and Alexander Disease Study Group in Japan. (2011). Nationwide survey of Alexander disease in Japan and proposed new guidelines for diagnosis. J. Neurol. 258,1998-2008.

Accepted April 3, 2019